

Learning a Unified Degradation-aware Representation Model for Multi-modal Image Fusion

Haolong Ma
Jiangnan University

Hui Li
Jiangnan University

Chunyang Cheng
Jiangnan University

Zeyang Zhang
Jiangnan University

Zhongwei Shen
Jiangsu University of Science and Technology

Xiaoning Song
Jiangnan University

Xiao-Jun Wu
Jiangnan University

Abstract

All-in-One Degradation-Aware Fusion Models (ADFMs), a class of multi-modal image fusion models, address complex scenes by mitigating degradations from source images and generating high-quality fused images. Mainstream ADFMs often rely on highly synthetic multi-modal multi-quality images for supervision, limiting their effectiveness in cross-modal and rare degradation scenarios. The inherent relationship among these multi-modal, multi-quality images of the same scene provides explicit supervision for training, but also raises above problems. To address these limitations, we present LURE, a Learning-driven Unified REpresentation model for infrared and visible Image Fusion, which is degradation-aware. LURE decouples multi-modal multi-quality data at the data level and recouples this relationship in a unified latent feature space (ULFS) by proposing a novel unified loss. This decoupling circumvents data-level limitations of prior models and allows leveraging real-world restoration datasets for training high-quality degradation-aware models, sidestepping above issues. To enhance text-image interaction, we refine image-text interaction and residual structures via Text-Guided Attention (TGA) and an inner residual structure. These enhances text’s spatial perception of images and preserve more visual details. Experiments show our method outperforms state-of-the-art (SOTA) methods across general fusion, degradation-aware fusion, and downstream tasks. The code will be publicly available.

1. Introduction

Multi-modal image fusion, aims at creating high-quality fused images by integrating multi-modal sensor data; notably, infrared and visible image fusion is recognized as one of its crucial tasks [16, 26, 61]. It faces challenges due to degradations in visual information of different modalities.

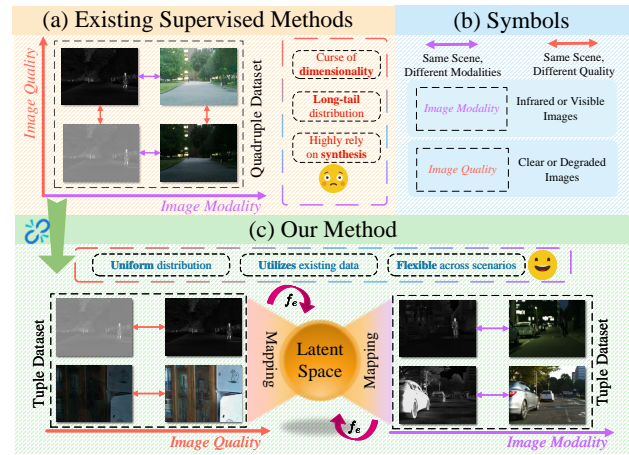


Figure 1. Mechanisms of Existing Supervised Methods vs. Our Method. (a) Existing methods commonly utilize datasets constructed with quadruplets (*i.e.* 4 images, same scene, varying modalities & qualities), which introduces a series of issues. (b) Legend for symbols. (c) Our method disentangles this quadruplets at the data level and re-associates it in the feature space, thus achieving greater flexibility and versatility.

Detailed visible images degrade under varying weather and lighting, causing information loss. In contrast, infrared images, capturing thermal radiation in adverse environments, typically have lower resolution/contrast.[30, 56, 58]. Thus, effective degradation removal and complementary data integration are essential for accurate scene reconstruction [8].

A conventional two-step approach initially employs SOTA restoration models for modality-specific degradation removal, followed by fusion models for complementary information integration [56]. However, this strategy often results in domain shift due to the domain discrepancy between restoration and fusion models. Moreover, degradation combinations from both modalities, *e.g.*, low light for visible images and low contrast for infrared images, will increase

the challenge, rendering separate fusion model training for each degradation combination infeasible [9, 25, 62].

Current methods address this problem in one step by training an All-in-One degradation-aware fusion model (ADFM). Mainstream ADFMs typically employ a supervised paradigm, relying on high-quality paired infrared and visible images as explicit supervisory signals to achieve high-quality fusion [10, 56]. However, these methods exhibit limited generalization to combined degradations and over-rely on synthetic data. Some unsupervised ADFMs address these issues [14]; for instance, DAFusion [48] utilizes contrastive learning and unpaired references, demonstrating improved generalization. Nevertheless, unsupervised methods often result in inferior fusion quality with detail loss due to the absence of explicit high-quality supervision.

To address these issues, analyzing image properties is crucial. Images are often characterized by modality and quality. Fig.1 (a) shows these dimensions form a coupled data quadruplet. Quality-wise, each modality requires paired low/high-quality images. Modality-wise, each image requires a cross-modality counterpart. This coupling causes two key issues: (1) High-quality restoration datasets become unusable due to lacking modality counterparts; (2) Sparse cross-modality degradation combinations lead to the “curse of dimensionality”. Furthermore, fusion datasets exhibit long-tailed degradation distributions, making crucial degradation synthesis challenging, *e.g.*, fog needs depth maps [1, 40, 47].

The aforementioned problems stem from modality and quality coupling. While it facilitates end-to-end fusion and circumvents domain shift, it also introduces data-level challenges. As shown in Fig.1 (c), we address these by decoupling the quadruplets at the data-level, mapping data to a unified latent feature space (ULFS) that transforms needed data into binary tuples for restoration and fusion, thereby benefiting from a substantial amount of high-quality existing data, *e.g.*, RESIDE [18], LOL [51], etc.

Fig.1 (c) shows these independent datasets sharing a latent space via mapping operation. Within this space, feature-level degradation combination becomes feasible, obviating data-level degradation combination concerns. However, the input-output residual connections of conventional restoration models, designed for better convergence, can also hinder latent representation learning by prioritizing degradation removal over source reconstruction [6, 7, 20, 57]. To counter this, we introduce a novel structure for efficient latent representation learning, named as inner-residual. Finally, we integrate text for flexible user control. To improve text-image feature interaction, we advance beyond simple channel weighting with Text-Guided Attention (TGA), enhancing text awareness spatially and channel-wise. The contributions of this paper can be summarized as follows:

- A novel data-decoupling and feature association method is proposed to address challenges in synthetic data over-reliance and jointly handle cross-model combined degradations.

- An efficient inner residual structure and a text-image interaction mechanism are introduced to enhance the semantic interaction ability through textual conditioned latent feature representations.

- Extensive experiments are conducted. Results demonstrate the effectiveness of the proposed approach.

2. Related Work

2.1. Recent Image Fusion Methods

Mainstream image fusion models fall into three categories: generative models (*e.g.*, FusionGAN, DDFM)[32, 33, 64], end-to-end approaches (*e.g.*, U2Fusion)[27, 42, 63], and autoencoder-based methods (*e.g.*, DenseFuse)[22–24]. Generative models fuse images via distribution approximation, yet face training instability and heuristic designs. End-to-end methods directly derive fused images, constrained by designed loss functions. Despite stable training, their generalization is limited by handcrafted loss functions. Early autoencoders lacked adaptability with hand-engineered fusion strategies[22], whereas current methods use learnable rules for better adaptation[23]. Autoencoder methods inherently decouple fusion rule and feature learning, facilitating versatile, degradation-aware paradigms.

2.2. All-in-One Degradation-aware Models

All-in-One Degradation-aware Models (ADM) address diverse degradations within a single model[10, 20, 21]. In image restoration field, ADMs benefit from abundant high-quality datasets and use techniques like prompt/continual learning[1, 18, 51].

However, in image fusion field, ADFMs face challenges due to long-tailed degradation distributions in fusion datasets, lacking sufficient data for robust degradation restoration[31, 41, 54, 56]. Unsupervised methods like contrastive learning exist but often yield lower quality due to lacking explicit supervision[48]. Current ADFMs still rely on existing fusion dataset degradations or synthetic ones, which may not match real degradation distributions[48, 56]. Some degradations require extra modality information for realistic synthesis (*e.g.*, fog needs depth maps), which is unavailable in current datasets.

These limitations hinder the generalization of current ADFMs. To address the above drawbacks, we propose a unified degradation-aware representation model to decouple image restoration and fusion data-level and re-associate them in latent space, which allows leveraging high-quality image restoration data to overcome current ADFMs challenges.

3. Proposed Method

3.1. Problem Formulation

In this paper, low/high-quality images are denoted by sets \mathcal{X}/\mathcal{Y} . Infrared/visible images are denoted by sets \mathcal{I}/\mathcal{V} .

Assume the set \mathcal{X} of T degradation types. For the t -th degradation ($t \in \{1, 2, \dots, T\}$), let c_t denote its description (e.g., text embedding), with $c_t \in \mathcal{C}$ and $\mathcal{C} = \{c_t\}_{t=1}^T$. Theoretically, for each image $x \in \mathcal{X}$, there exists a deterministic mapping to a corresponding degradation description c_t .

For supervised method, samples are quadruplets $(x_{ir}, y_{ir}, x_{vi}, y_{vi})$, where ir/vi denote infrared/visible modalities, and x/y are low/high-quality images. Define modality-paired sets: \mathcal{I}_g (infrared), \mathcal{V}_g (visible):

$$\mathcal{I}_g = \{(x_{ir}, y_{ir}) \mid x_{ir} \in \mathcal{X}, y_{ir} \in \mathcal{Y}, y_{ir} = f(x_{ir})\} \quad (1)$$

where f maps low-quality images to clean counterparts. \mathcal{V}_g is defined analogously.

Given a sample $(x_{ir}, y_{ir}, x_{vi}, y_{vi})$ from the joint distribution $P_{\mathcal{I}_g, \mathcal{V}_g}(x_{ir}, y_{ir}, x_{vi}, y_{vi})$ and the description c , the loss function of existing supervised methods can be expressed as $\mathcal{L}_{if}(y_{ir}, y_{vi}, \mathcal{F}_{if}(x_{ir}, x_{vi}, c; \theta))$ where, \mathcal{L}_{if} is the fusion loss. \mathcal{F}_{if} is a network parameterized by θ , fusing degraded infrared and visible images with degradation description c .

Such supervised approaches necessitate quadruplet samples from the joint distribution of \mathcal{I}_g and \mathcal{V}_g to provide supervision signals. This leads to the curse of dimensionality in handling combined degradations, fundamentally due to coupling modalities and quality dimensions at the data level.

3.2. Data Decoupling and Feature Association

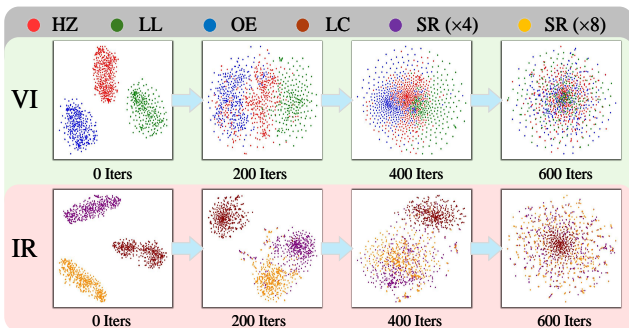


Figure 2. T-SNE visualization of ULFS distributions for tasks (e.g., HZ denotes Dehaze; other abbreviations are detailed in Sec.4.1.1.) of both modalities across training iterations. It reveals initial distinct task distributions gradually merging into a unified distribution. Detailed t-SNE visualizations are in the supplementary material.

To address modality-quality coupling in data-level, a novel decoupling mechanism which still preserves inherent

associations of source data is needed. We thus propose a ULFS (\mathcal{Z}) to re-establish these associations at feature level. Initially, we focus on image quality, disregarding modality, and define \mathcal{Z} as follows:

Definition: [Unified Latent Feature Space (\mathcal{Z})].

\mathcal{Z} is defined by mapping $f_e : \mathcal{X} \rightarrow \mathcal{Z}$, with conditions:

1. $\forall x \in \mathcal{X}, \exists z \in \mathcal{Z} (z = f_e(x))$.
2. $\forall z \in \mathcal{Z}, \forall c \in \mathcal{C} (P(c|z) = P(c))$.

1. Condition 1 ensures every degraded image maps to \mathcal{Z} .
2. Condition 2 ensures that for any latent feature $z \in \mathcal{Z}$, the posterior $P(c|z)$ distribution equals the prior $P(c)$ distribution for $c \in \mathcal{C}$.

Practically, each modality learns its own \mathcal{Z} for quality decoupling. These \mathcal{Z} properties guarantee f_e mapping eliminates unique degradation information. As shown in Fig.2, this ‘mixing’ of feature distributions in \mathcal{Z} renders degradations indistinguishable, allowing transfer of fusion rules across degradations.

We learn \mathcal{Z} for image quality using image restoration data at first stage. Then, at second stage, we learn a fusion rule in \mathcal{Z} using image fusion data.

However, fusion rule learning still necessitates a modality-quality coupled dataset to associate first and second stage at feature level, incompletely decoupling dimensions. To achieve full decoupling, we introduce a pseudo-degradation task that auto-encodes the input image, thereby transferring this coupling to it.

3.2.1. Unified Latent Representation Learning

Theoretically, to align with the definition of \mathcal{Z} for ULFS learning, we aim to minimize the distribution distance of degraded images within \mathcal{Z} . Learning Objective:

$$\min_{\theta} \sum_{t=1}^T \sum_{t' \neq t}^T \text{KL}(P_{\mathcal{Z}}^{(t)}(z) \parallel P_{\mathcal{Z}}^{(t')}(z)) \quad (2)$$

where, $\text{KL}(\cdot \parallel \cdot)$ denotes the Kullback-Leibler divergence, and $P_{\mathcal{Z}}^{(t)}(z)$ represents the distribution of the t -th degradation in \mathcal{Z} .

To minimize Eq.2, Generative Adversarial Networks (GANs) with discriminators are commonly used for adversarial training [28, 37]. However, inherent distribution differences exist across image restoration datasets. Discriminators capture these discrepancies, leading to suboptimal representation learning for f_c and sensitive GAN training, hindering model convergence.

To mitigate this issue, we introduce a pseudo-degradation task. This task, fundamentally image reconstruction, is not a genuine degradation. For this task, pseudo-degradation data pairs (x, y) satisfy $x = y$, where $x \in \mathcal{X}$ and $y \in \mathcal{Y}$. We control this task via a description

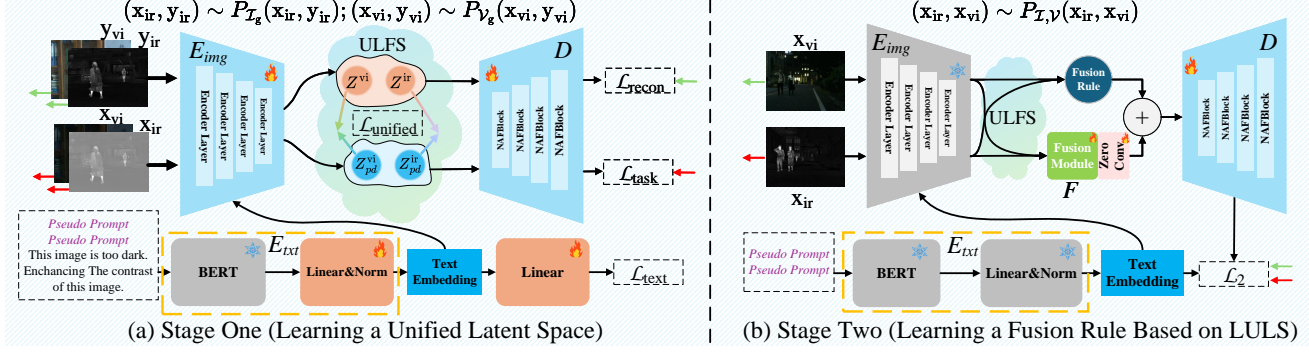


Figure 3. Schematic diagram of the two-stage training process. (a) In the first stage, a unified latent feature space is learned under the guidance of text. (b) In the second stage, all encoders are frozen, a fusion module is incorporated to learn a fusion strategy. ‘pseudo prompt’ refers to the dedicated prompt for the pseudo degradation and the detailed information of it can be found in supplementary materials.

c_{pd} and align all degradation distributions to this pseudo-degradation task distribution. However, directly computing Kullback-Leibler divergence between tasks is challenging, requiring optimization objective transformation.

For the t -th degradation, given an image restoration data pair (x_t, y_t) where $x_t \in \mathcal{X}$ and $y_t \in \mathcal{Y}$, we have $z_t = f_e(x_t, c_t)$. We construct a pseudo-task data pair (y_t, y_t) , yielding $z_{pd} = f_e(y_t, c_{pd})$.

Theoretically, z_{pd} should ideally correspond to z_t as a feature point in ULFS. This is justified by:

1. x_t and y_t represent the same scene information.
2. Pseudo-degradation, being image reconstruction of degradation-free y_t , results in $z_{pd} \in \mathcal{Z}$ lacking degradation information, thus obscuring original degradation types.

Therefore, to align distributions of tasks in \mathcal{Z} , we ensure each task’s representation aligns with its pseudo-task counterpart. We transform distribution alignment in the objective function to feature alignment:

$$\mathcal{L}_{\text{unified}} = \frac{1}{T} \sum_{t=1}^T \{1 - \Gamma[f_e(X_t, c_t), f_e(Y_t, c_{pd})]\} \quad (3)$$

where, X_t and Y_t represent low-quality and high-quality image datasets for task t , respectively. Γ measures feature distances in \mathcal{Z} , employing cosine similarity.

Directly constraining feature relationships for \mathcal{Z} learning is more stable than GAN-based adversarial methods. The pseudo-task serves as an image auto-encoding task to learn a fusion rule in the second stage and associate two stages at feature level. In practice, f_e is a conditional image encoder.

3.3. Network Pipeline

In this section, the details of our model architecture are introduced, including Encoders (E_{img} and E_{txt}), Fusion Module (F), and Decoder (D). Then, we describe two-stage training and loss function. Finally, the end-to-end inference for diverse scenarios is presented.

3.3.1. Encoder and Decoder Structure

As shown in Fig.3 (a), the encoder is bifurcated into image (E_{img}) and text (E_{txt}) encoders. E_{txt} employs Distilled BERT [13], with a Norm layer and a Linear layer to project its final output into a text feature vector. A classification head and cross-entropy loss (\mathcal{L}_{txt}) are used to align task categories for each task-specific text feature vector, an approach effective in InstructIR and superior to the CLIP text encoder [38].

E_{img} consists of multi-scale Encoder Layers. Learning \mathcal{Z} requires effective mapping and reconstruction of the input image. Conventional image restoration models often utilize a residual structure ($\hat{y} = \mathcal{M}(x) + x$), where \hat{y} represents the predicted high-quality image, x is the low-quality input, and \mathcal{M} is the restoration model [6, 20, 57]. This approach, however, prioritizes learning degraded regions over source image reconstruction, which may not suitable for learning \mathcal{Z} in our framework.

Since directly eliminating the residual branch may lead to detail loss, we designed an inner residual structure to preserve details as much as possible. Each Encoder Layer (Fig.4) comprises four modules: BaseBlock, TGABlock (Text-Guided Attention Block), BottleNeck, and Linear. The TGABlock is combined with BaseBlock and BottleNeck to form two composite modules. Each module iterates K_{tb}^i and K_{tb}^i times in the i -th layer.

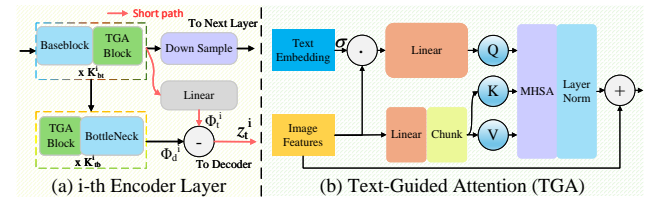


Figure 4. Schematic diagrams of Encoder and Text-Guided Attention (TGA). (a) Structure diagram of the Encoder Layer. (b) Structure diagram of TGA. “ \odot , \oplus , \ominus ” represent Element-wise operations, and σ represents the Sigmoid function.

As shown in Fig.4 (a), at the i -th layer, TGABlock + BaseBlock extract modality-specific image information and initially integrate degradation information, guided by text. It's output then branch into three paths: (1) direct down-sampling to next layer; (2) degradation-specific information Φ_d^i extraction via TGABlock + BottleNeck; (3) task-relevant base information Φ_t^i filtering by a linear layer. Subsequently, a residual operation subtracts degradation-specific information Φ_d^i from task-relevant base information Φ_t^i , yielding task-irrelevant latent representations: $z_t^i = \Phi_t^i - \Phi_d^i$. This inner residual connection provides a shorter path to decoder, preventing detailed information loss.

BaseBlock, consisting of NAFBlock [6] and Modality Embedding, serves to extract modality-specific basic information from images. The BottleNeck module, comprising a NAFBlock and a 1×1 convolution, is designed to preserve text-relevant features and reduce redundant channels following the TGABlock.

For image-text interaction, the TGABlock utilizes a Transformer-like architecture, using GDFN (gated-Dconv FN) as the feed forward block [57]. In contrast to conventional methods that passively weight image channels with text [36, 56], which limits the global attention of text, our TGABlock can avoid this drawback.

As illustrated in Fig.4 (b), we use channel-weighted text information as the Query to proactively attend to global image features. These enhances text's spatial perception of images and preserve more task-related visual information.

Each decoder layer upsamples and simply employs few NAFBlocks to progressively reconstruct image details from \mathcal{Z} . For fusion task, a highly effective mechanism, cross attention, is used. Multiple Cross Attention modules are utilized at each scale.

3.3.2. Training

In our proposed framework, the training processing is a two-stage scheme. As shown in Fig.3 (a), in the first stage, the latent space \mathcal{Z} is learned. For each sample, we have $(x_{ir}, y_{ir}) \sim P_{\mathcal{I}_g}(x_{ir}, y_{ir})$ or $(x_{vi}, y_{vi}) \sim P_{\mathcal{V}_g}(x_{vi}, y_{vi})$. To explicitly represent modality information, we transform the data into triplets (x, y, m) , where $m \in \{0, 1\}$; 0 denotes visible modality, and 1 denotes infrared modality.

As shown in Fig.3 (b), stage two learns fusion rules. Input pairs are (x_{ir}, x_{vi}) from image fusion datasets: $(x_{ir}, x_{vi}) \sim P_{\mathcal{I}, \mathcal{V}}(x_{ir}, x_{vi})$.

Stage one uses image restoration datasets, stage two uses an image fusion dataset.

First stage training: In first stage, the unified latent space, \mathcal{Z} , is learned. Image and text encoders extract multi-scale features for both real and pseudo-task data. Given low-quality image x , high-quality image y , text ω , description $c_t = E_{\text{txt}}(\omega)$, pseudo-task text ω_{pd} , pseudo description $c_{pd} = E_{\text{txt}}(\omega_{pd})$, and modality m . We extract latent features: $Z = E_{\text{img}}(x, c_t, m)$ and $Z_{pd} = E_{\text{img}}(y, c_{pd}, m)$

where Z, Z_{pd} are multi-scale latent representations. The decoder reconstructs images: $\hat{y} = D(Z)$ and $\hat{y}_{pd} = D(Z_{pd})$.

The first stage loss \mathcal{L}_1 is formulated as follows:

$$\mathcal{L}_1 = \mathcal{L}_{\text{task}} + \alpha_1^{(1)} \mathcal{L}_{\text{unified}} + \alpha_2^{(1)} \mathcal{L}_{\text{recon}} + \alpha_3^{(1)} \mathcal{L}_{\text{text}} \quad (4)$$

where,

1. $\mathcal{L}_{\text{recon}} = \|\hat{y}_{pd} - y\|_1$ represents the reconstruction loss for the pseudo-degradation task.
2. $\mathcal{L}_{\text{task}} = \|\hat{y} - y\|_1 + \alpha_{\text{task}} \|\|\nabla \hat{y}\| - \|\nabla y\|\|_1$ represents the loss for different degradation tasks (∇ : Sobel operator)
3. $\mathcal{L}_{\text{unified}} = 1 - \Gamma(Z, Z_{pd})$, (Γ : Cosine Similarity)
4. $\alpha_1^{(1)}, \alpha_2^{(1)}, \alpha_3^{(1)}, \alpha_{\text{task}}$ are hyperparameters.

Second stage training: In second stage, the proposed model learns fusion rules based on \mathcal{Z} . Given an infrared image x_{ir} , visible image x_{vi} , the pseudo-degradation prompt ω_{pd} and pseudo-degradation task description ($c_{pd} = E_{\text{txt}}(\omega_{pd})$), we extract latent features:

$$Z_{pd}^{\text{ir}} = E_{\text{img}}(x_{ir}, c_{pd}, 1), \quad Z_{pd}^{\text{vi}} = E_{\text{img}}(x_{vi}, c_{pd}, 0) \quad (5)$$

Fusion result O_{fused} is obtained via:

$$O_{\text{fused}} = D\{\text{zero}[F(Z_{pd}^{\text{vi}}, Z_{pd}^{\text{ir}})] + \text{rule}(Z_{pd}^{\text{vi}}, Z_{pd}^{\text{ir}})\} \quad (6)$$

Inspired by ControlNet [59], we first implement a prior fusion rule, $\text{rule}(\cdot, \cdot)$, for initial feature fusion. A learnable module, $F(\cdot, \cdot)$, then refines rule-based fusion results. A zero-initialized 1×1 convolution mitigates random initialization noise and accelerates Second Stage convergence.

The Second Stage loss function is defined as follows:

$$\mathcal{L}_2 = \mathcal{L}_{\text{color}} + \alpha_1^{(2)} \mathcal{L}_{\text{grad}} + \alpha_2^{(2)} \mathcal{L}_{\text{per}} \quad (7)$$

where $\alpha_1^{(2)}$ and $\alpha_2^{(2)}$ are hyperparameters balancing loss contributions. Since the proposed unified latent space can extract powerful degradation irrelevant features, theoretically, the fusion loss function not need to be specially designed. Thus, the color consistency item ($\mathcal{L}_{\text{color}}$) and gradient item ($\mathcal{L}_{\text{grad}}$) are chosen from Text-IF. The perceptual item (\mathcal{L}_{per}) is chosen from U2Fusion.

3.3.3. Inference

For inference with infrared and visible images (x_{ir}, x_{vi}) and degradation description $c_t = E_{\text{txt}}(\omega)$ and pseudo-degradation $c_{pd} = E_{\text{txt}}(\omega_{pd})$ (assuming infrared is degraded), the process of LURE is given as follows:

$$Z_{pd}^{\text{vi}} = E_{\text{img}}(x_{vi}, c_{pd}, 0), \quad Z_t^{\text{ir}} = E_{\text{img}}(x_{ir}, c_t, 1) \quad (8)$$

$$O_{\text{fused}} = D\{\text{zero}[F(Z_{pd}^{\text{vi}}, Z_t^{\text{ir}})] + \text{rule}(Z_{pd}^{\text{vi}}, Z_t^{\text{ir}})\} \quad (9)$$

Our End-to-end inference uses a single model. In degradation description, non-degraded and degraded modalities

are c_{pd} and c_t , respectively. This enables diverse degradation handling via modality-specific conditions, crucially addressing combined degradations through description combination, even without combined degradation training data.

Notably, our model do not complicates fusion process. Affected modalities are readily identified from user input via a simple text classification or regular expressions, allowing straightforward degradation description.

4. Experiment

4.1. Setting

In the proposed model, the encoder and the decoder both consist of 4 layers. The channel numbers for each layer are [48, 96, 192, 384], reduced to [16, 32, 64, 128] for each encoder layer’s output size. K_{bt} and K_{tb} are set to [1,1,2,2] and [2,2,4,8], respectively. Decoder blocks and fusion blocks for each layer is set to [1,1,1,1] and [1, 1, 2, 2]. The number of attention heads for TGA is set to 4, and the prior rule is selected from DenseFuse [22].¹

4.1.1. Training Data

For the first stage of training, we utilize the most common tasks for infrared modality: low contrast (LC) and low resolution (SR) ($\times 4$ and $\times 8$). We use the EMS Full dataset [56] and construct a high-quality super-resolution dataset on LLVIP [15], following the approach in InstructIR [36].

For visible modality, we perform dehazing (HZ), overexposure correction (OE), and low-light enhancement (LL). The high-quality images are chosen from the RESIDE [18], Exposure-Errors [1], and LOL datasets [51], respectively.

For the second stage, the training data of the MSRS datasets [41] is used. All of the aforementioned datasets are publicly available.

All task texts are generated by LLaMA [44].

4.1.2. Evaluation Data

For vanilla image fusion, we evaluate the fusion performance on the RoadScene [54], M3FD [41], TNO [43], and MSRS [41] test dataset.

For degradation-aware image fusion, we use EMS-full [56] for low contrast, overexposure correction, and low-light enhancement. We also construct a super-resolution test dataset on M3FD [41] in the same manner. For dehazing, we collect hazy samples from M3FD [41] to create a real-world dehazing test dataset.

For cross-modal combined degradations, we exemplify with low contrast + overexposure correction and low contrast + low light enhancement, creating combined test datasets from single modality degradation tasks.

¹More detailed hyperparameter (e.g. hyperparameter ablation) and training settings are provided in the supplementary materials.

4.1.3. Evaluation Metrics

The evaluation metrics include Correlation Coefficient (CC) [12], Spatial Correlation of Differences (SC) [4], Structural Similarity Index (SS) [49], Peak Signal-to-Noise Ratio (PS), Multiscale Structural Similarity (MS) [50], Average Gradient (AG), Standard Deviation (SD), Spatial Frequency (SF), Entropy (EN) [39], CLIP-IQA (CL) [45], LIQE (LI) [60], MANIQA (MA) [55], NIQE (NI) [35], NUSIQ [17] (NU), and ARNIQA (AR) [2].

These metrics comprehensively evaluate the fused image quality from multiple perspectives, including image noise, texture details, and preservation of source image structure. CLIP-IQA [45], LIQE [45], MANIQA [55], NUSIQ [17], and ARNIQA [2] are state-of-the-art no-reference image quality assessment metrics. Except for NIQE, higher values indicate better fusion quality.

4.2. SOTA Competitors

We conducted comparisons against seven state-of-the-art (SOTA) methods, including DCINN (DCI) [46], Fusion-Booster (FuB) [8], CSCFuse (CSC) [65], MMDRFuse (MMD) [11], Text-IF (TIF) [56], DAFusion (DAF) [48], and GTMFuse (GTM) [34]. Among these, Text-IF and DAFusion are categorized as All-in-One degradation-aware image fusion models.

4.3. Vanilla Image Fusion

Table 1. Quantitative comparison of vanilla image fusion task on MSRS and M3FD. Bold/underlined values: best/second best results.

Methods	MSRS [41]					M3FD [31]				
	CC	SC	PS	SS	MS	CC	SC	PS	SS	MS
DCI’23	0.58	1.49	<u>32.54</u>	0.36	0.45	0.59	1.37	<u>31.97</u>	<u>0.49</u>	0.49
CSC’23	0.53	0.92	31.83	0.16	0.28	0.58	1.67	30.47	0.43	0.48
MMD’24	0.61	1.53	32.47	<u>0.48</u>	0.52	0.62	1.40	31.13	0.49	<u>0.50</u>
GTM’24	0.60	1.61	31.64	0.42	0.50	0.59	1.52	30.34	0.24	0.41
FuB’25	0.67	1.53	31.2	0.34	0.50	0.59	1.53	29.61	0.40	0.47
TIF’24	0.60	<u>1.68</u>	32.29	0.48	<u>0.52</u>	0.58	1.41	31.67	0.48	0.48
DAF’25	<u>0.66</u>	1.58	28.80	0.26	0.41	<u>0.63</u>	1.75	30.51	0.42	0.46
LURE	0.61	1.74	32.56	0.49	0.53	0.64	<u>1.68</u>	32.12	0.50	0.53

Table 2. Quantitative comparison of vanilla image fusion task on TNO and RoadScene. Bold/underlined values: best/second best results.

Methods	TNO [43]					RoadScene [54]				
	CC	SC	PS	SS	MS	CC	SC	PS	SS	MS
DCI’23	0.42	1.61	<u>31.81</u>	0.29	0.36	0.56	1.16	<u>31.49</u>	0.16	0.36
CSC’23	0.44	<u>1.72</u>	30.49	0.44	<u>0.45</u>	0.63	1.80	30.82	0.46	0.52
MMD’24	0.46	1.59	31.18	<u>0.48</u>	0.43	<u>0.63</u>	1.10	31.27	0.41	0.48
GTM’24	0.45	1.68	30.46	0.37	0.41	0.60	1.55	29.55	0.33	0.45
FuB’25	0.46	1.54	29.07	0.40	0.42	0.59	1.03	29.39	0.35	0.45
TIF’24	0.42	1.67	31.29	0.47	0.44	0.61	1.57	31.21	0.48	0.52
DAF’25	0.49	1.70	30.53	0.44	0.41	0.64	1.65	31.34	<u>0.48</u>	<u>0.53</u>
LURE	<u>0.46</u>	1.84	31.92	0.51	0.47	0.57	<u>1.67</u>	31.52	0.50	0.55

To ensure fair comparison, we first tested degradation-unaware fusion tasks. Quantitative results are in Tab.1

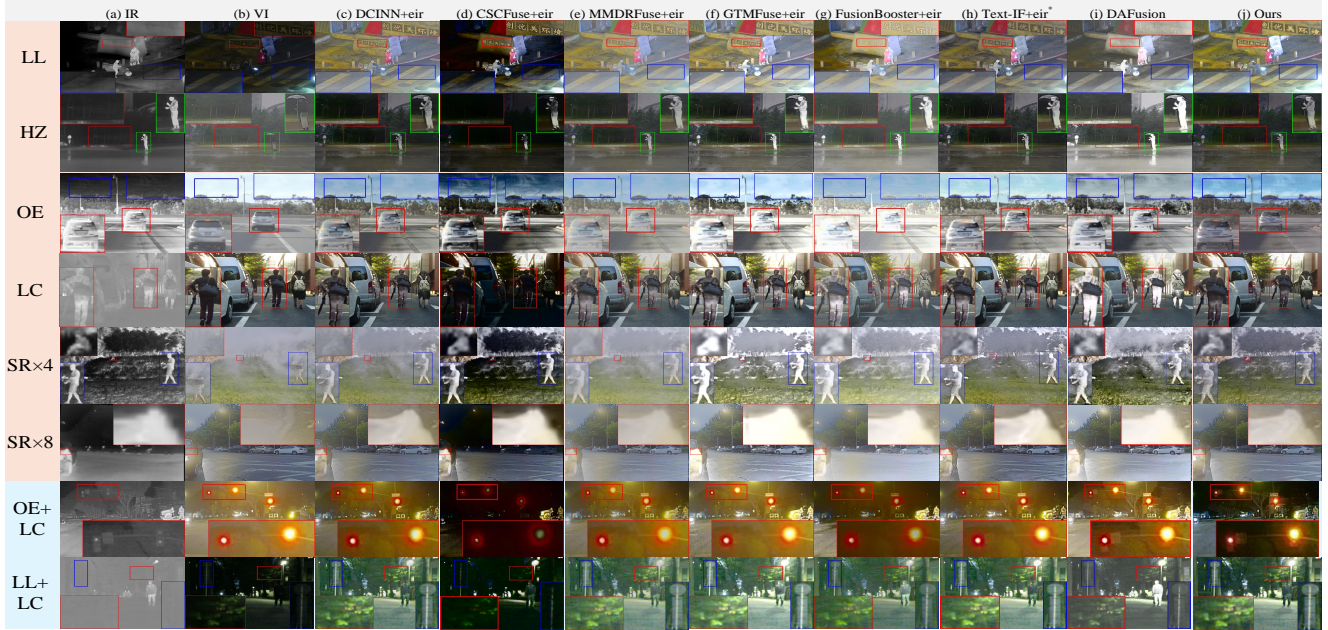


Figure 5. Qualitative comparison of degradation-aware fusion tasks: Low Light (LL), Dehaze (HZ), Overexposure (OE), Low Contrast (LC), Super Resolution (SR4, SR8), Overexposure for visible images/Low Contrast for infrared images (OE+LC), Low Light for visible images/Low Contrast for infrared images (LL+LC), and Low Contrast (LC). “eir” denotes External Image Restoration Methods. Text-IF uses “eir” only for Super Resolution and combined degradations. For more detail about the qualitative comparison, please refer to supplementary materials.

and Tab.2. Our method achieves SOTA across all datasets, demonstrating superior performance. Leveraging high-quality image restoration datasets, our method attains higher PS (PSNR), indicating less noisy fusion results. Furthermore, Inner Residuals help preserve more source information, leading to better CC and SC (SCD), and improved SS/MS (SSIM/MS-SSIM), signifying better source information retention and structural fidelity at multiple scales.

4.4. Degradation-aware Image Fusion

Table 3. Quantitative comparison of degradation-Aware fusion tasks: Low Light Enhancement (LL), Dehaze (HZ), Overexposure Correction (OE), and Low Contrast Enhancement (LC). Bold/underlined values: best/second best results. † denotes All-in-One type methods.

Method	LL			HZ			OE			LC		
	AG	SD	CL	CL	LI	AR	CL	LI	MA	CL	MA	NI ↓
DCI'23	4.74	40.90	<u>0.19</u>	0.21	<u>1.17</u>	0.52	0.19	1.26	0.22	0.14	0.14	4.74
CSC'23	4.27	<u>51.08</u>	0.17	0.25	1.09	0.51	0.19	1.38	<u>0.24</u>	0.12	0.12	6.38
MMD'24	3.95	36.07	0.15	0.23	1.17	0.53	0.19	1.23	0.24	0.14	0.14	4.55
GTM'24	4.15	50.75	0.12	0.18	1.01	0.36	0.14	1.05	0.16	0.14	0.13	6.54
FuB'25	4.10	37.36	0.17	0.24	1.12	0.53	0.13	1.05	0.20	0.15	0.15	4.66
TIF'24 †	4.05	42.10	0.19	<u>0.25</u>	1.17	<u>0.53</u>	0.23	1.49	0.23	<u>0.16</u>	0.13	4.41
DAF'25 †	5.19	47.99	0.19	0.25	1.19	0.51	0.20	1.55	0.24	0.13	0.10	3.17
LURE †	4.77	55.23	0.20	0.30	1.14	0.54	0.21	1.37	0.25	0.17	0.14	4.67

²For qualitative evaluation results, due to page limitations, please refer to the supplementary materials.

Table 4. Quantitative comparison of degradation-aware fusion tasks: Super Resolution (SR4, SR8), Overexposure for visible images/Low Contrast for infrared images (OE+LC), Low Light for visible images/Low Contrast for infrared images (LL+LC). Bold/underlined values: best/second best results. † denotes All-in-One type methods.

Method	SR4			SR8			OE+LC			LL+LC		
	SF	CL	AR	SF	CL	AR	SD	NU	CL	EN	SD	CL
DCI'23	10.09	0.26	0.58	10.15	0.24	0.56	42.46	5.85	0.20	7.10	42.46	<u>0.13</u>
CSC'23	<u>14.23</u>	0.28	0.59	<u>13.16</u>	0.25	0.57	47.61	4.20	0.15	5.88	47.61	0.11
MMD'24	9.22	0.29	<u>0.59</u>	9.36	0.25	0.57	37.44	4.98	0.21	6.93	37.44	0.10
GTM'24	8.76	<u>0.32</u>	0.37	8.65	0.29	0.35	<u>53.00</u>	6.36	0.15	7.23	<u>53.00</u>	0.10
FuB'25	9.13	0.28	0.58	9.16	0.24	0.57	34.39	5.57	0.16	6.88	34.39	0.11
TIF'24 †	13.20	0.26	0.59	12.78	0.23	0.57	49.43	6.86	<u>0.23</u>	7.26	49.43	0.12
DAF'25 †	15.23	0.22	0.57	15.23	0.24	<u>0.58</u>	52.56	6.37	0.20	7.24	50.84	0.11
LURE †	11.20	0.33	0.60	9.77	<u>0.27</u>	0.59	55.40	<u>6.84</u>	0.24	7.42	55.40	0.15

Degradation-aware fusion demands models to eliminate degradations and integrate valid source information.

For fair comparison, we use a two-step strategy for degradation-unaware methods: SOTA external image restoration followed by image fusion. For Text-IF's limitations on some tasks, e.g., super-resolution and combined degradation, we also use this two-stage approach on these tasks. In addition, DCINN [46], FusionBooster [46], CSC-Fuse [65], MMDRFuse [11], and GTMFuse [34] all employ a two-step strategy across tasks. Task-specific SOTA image restoration models: URetinex (low-light) [52], SGID-PFF (dehazing) [5], CoTF (overexposure) [29], AirNet (low con-

trast) [19], SwinFuSR (super-resolution) [3].³

4.4.1. Qualitative Comparison

Fig.5 qualitatively compare LURE with SOTA methods across degradations, showing LURE’s superiority.

Unlike the existing all-in-One method (DAFusion [48]), LURE benefits from explicit labels as supervisory signals, resulting in richer textural details and less noise in fusion outcomes. Compared to Text-IF [56], our method unconstrained by quadruple data format, leverages more high-quality image restoration datasets with real-world scenarios, and yielding more natural images without pre-enhanced sources. Against two-step models like CSCFuse [65] or MMDRFuse [11], LURE reduces domain shift-related degradation and information loss.

More crucially, consistent with DAFusion, our method inherently addresses cross-modal combined degradations, achieving superior performance without supplementary combined degradation training datasets. Text-IF, method-limited, struggles with combined degradations, thus needs external restoration, yielding lower quality. Specifically, for OE+LC and LL+LC tasks, our method exhibits superior texture detail, color vividness, and contrast compared to other approaches. This highlights our method’s ability to attain high-quality fused images without additional restoration models or even combined degradation training datasets.

4.4.2. Quantitative Comparison

Tab.3 and Tab.4 quantitatively compares LURE and SOTA methods across degradations.

LURE generally achieves SOTA performance in 8 tasks. Higher EN, AG, SD, and SF metrics show LURE preserves textural details and clarity. Concurrently, CLIP-IQA (CL), ARNIQA (AR), NUSIQ (NU), MANIQA (MA), LIQE (LI), and NIQE (NI) scores indicate less noise and improved perceptual quality, better aligning with human vision.

4.5. Multi-modal Semantic Segmentation

To assess the effectiveness of LURE in high-level tasks, the experiment of multi-modal semantic segmentation is conducted. Segformer-b2 [53] is fine-tuned on MSRS fusion results and evaluated on the test dataset⁴.

Tab.5 presents mIOU scores, showing LURE achieves SOTA segmentation performance, demonstrating visual efficacy on salient objects. Fig.6 illustrates LURE preserves more texture details than other approaches, enabling more accurate boundary delineation and improved segmentation.

4.6. Ablation Study

To validate the effectiveness of our proposed framework, several ablation studies are conducted (Tab.6), including:

³For more information including prompts used in experiments, please refer to supplementary materials.

⁴For more details please refer to supplementary material.

Table 5. Quantitative comparison of multi-modal semantic segmentation on MSRS. Bold/underlined values: best/second best results.

	IR	VI	DCI	CSC	MMD	GTM	FuB	TIF	DAF	LURE
mIOU	77.679	78.94	<u>80.05</u>	77.2	78.87	79.4	78.84	78.21	79.1	81.22

Figure 6. Qualitative comparison of multi-modal semantic segmentation on “00734N” image of MSRS.

Single Stage training, Using CC (vs. Cosine Similarity), w/o Inner Residual, TGA→Gate, w/o Unified Loss and w/o Rule⁵.

Ablation results show Single Stage training caused learning difficulties due to conflicting losses. TGA→Gate substitution impairs spatial information perception from images with text guidance. ‘w/o Unified Loss’ hinders \mathcal{Z} learning, significantly degrading fusion quality across tasks.

In remaining ablations, ‘w/o Inner Residual’ makes model prone to high-frequency information loss and convergence issues (minor impact). ‘w/o Rule’ slows Stage Two convergence (moderate impact). Conversely, ‘Using CC’, it provides weaker spatial constraints than Cosine Similarity, caused fusion rule transferability issues.

Table 6. Ablation Studies on Low Contrast Enhancement (LC), Overexposure (OE), and Low Light Enhancement and Contrast Enhancement for infrared and visible images tasks respectively (LL+LC). Bold/underlined values: best/second best results.

	LC			OE			LL+LC		
	CL	MA	NI ↓	CL	LI	MA	EN	SD	CL
Single Stage	0.168	0.135	4.397	0.205	1.041	0.207	6.473	36.901	0.149
Using CC	0.155	0.135	4.828	0.195	1.208	0.216	<u>7.230</u>	48.035	0.134
w/o Inner Residual	0.165	0.138	5.100	<u>0.206</u>	<u>1.310</u>	<u>0.244</u>	7.056	40.099	<u>0.149</u>
TGA→Gate	0.163	0.130	5.000	0.180	1.080	0.200	7.184	45.001	0.143
w/o Unified Loss	<u>0.169</u>	<u>0.139</u>	5.024	0.205	1.030	0.198	7.100	45.829	0.139
w/o Rule	0.159	0.133	5.168	0.203	1.236	0.227	7.053	<u>48.099</u>	0.136
Ours	0.170	0.141	<u>4.621</u>	0.212	1.374	0.251	7.422	55.403	0.150

5. Conclusion

This paper addresses limitations of prior ADFMs constrained by long-tailed data, dimensionality curse, and synthetic data reliance. By decoupling modality and quality dimensions at data level and reassociating it at ULFS, our proposed approach mitigates these issues, provides effective supervision, and yields superior fusion performance. Fur-

⁵For more detailed qualitative comparisons and hyperparameter ablation studies, please refer to the supplementary material.

thermore, an inner residual model and Text-Guided Attention (TGA) enhance spatial perception and detail preservation. Extensive experiments validate our proposed method achieves better performance in vanilla and degradation-aware fusion. Importantly, our method is applicable not only to infrared-visible image fusion but also to other multi-modal image fusion tasks. We believe our approach offers a fresh perspective and inspires future fusion research.

References

- [1] Mahmoud Afifi, Konstantinos G Derpanis, Bjorn Ommer, and Michael S Brown. Learning multi-scale photo exposure correction. In *Proceedings of the IEEE/CVF Conference on Computer Vision and Pattern Recognition*, pages 9157–9167, 2021. [2](#), [6](#)
- [2] Lorenzo Agnolucci, Leonardo Galteri, Marco Bertini, and Alberto Del Bimbo. Arniqa: Learning distortion manifold for image quality assessment. In *Proceedings of the IEEE/CVF Winter Conference on Applications of Computer Vision*, pages 189–198, 2024. [6](#)
- [3] Cyprien Arnold, Philippe Jouvét, and Lama Seoud. Swin-fusr: An image fusion-inspired model for rgb-guided thermal image super-resolution. In *Proceedings of the IEEE/CVF Conference on Computer Vision and Pattern Recognition (CVPR) Workshops*, pages 3027–3036, 2024. [8](#)
- [4] V Aslantas and Emre Bendes. A new image quality metric for image fusion: The sum of the correlations of differences. *Aeu-international Journal of electronics and communications*, 69(12):1890–1896, 2015. [6](#)
- [5] Haoran Bai, Jinshan Pan, Xinguang Xiang, and Jinhui Tang. Self-guided image dehazing using progressive feature fusion. *IEEE Transactions on Image Processing*, 31:1217 – 1229, 2022. [7](#)
- [6] Liangyu Chen, Xiaojie Chu, Xiangyu Zhang, and Jian Sun. Simple baselines for image restoration. In *European conference on computer vision*, pages 17–33. Springer, 2022. [2](#), [4](#), [5](#)
- [7] Xiangyu Chen, Zheyuan Li, Yuandong Pu, Yihao Liu, Jiantao Zhou, Yu Qiao, and Chao Dong. A comparative study of image restoration networks for general backbone network design. *arXiv preprint arXiv:2310.11881*, 2023. [2](#)
- [8] Chunyang Cheng, Tianyang Xu, Xiao-Jun Wu, Hui Li, Xi Li, and Josef Kittler. Fusionbooster: A unified image fusion boosting paradigm. *International Journal of Computer Vision*, pages 1–18, 2024. [1](#), [6](#)
- [9] Chunyang Cheng, Tianyang Xu, Xiao-Jun Wu, Hui Li, Xi Li, Zhangyong Tang, and Josef Kittler. Textfusion: Unveiling the power of textual semantics for controllable image fusion. *Information Fusion*, 117:102790, 2025. [2](#)
- [10] Marcos V Conde, Gregor Geigle, and Radu Timofte. Instructir: High-quality image restoration following human instructions. In *European Conference on Computer Vision*, pages 1–21. Springer, 2024. [2](#)
- [11] Yanglin Deng, Tianyang Xu, Chunyang Cheng, Xiao-Jun Wu, and Josef Kittler. Mmdrfuse: Distilled mini-model with dynamic refresh for multi-modality image fusion. In *Proceedings of the 32nd ACM International Conference on Multimedia*, pages 7326–7335, 2024. [6](#), [7](#), [8](#)
- [12] Manjusha Deshmukh, Udhav Bhosale, et al. Image fusion and image quality assessment of fused images. *International Journal of Image Processing (IJIP)*, 4(5):484, 2010. [6](#)
- [13] Jacob Devlin, Ming-Wei Chang, Kenton Lee, and Kristina Toutanova. Bert: Pre-training of deep bidirectional transformers for language understanding. In *Proceedings of the 2019 conference of the North American chapter of the association for computational linguistics: human language technologies, volume 1 (long and short papers)*, pages 4171–4186, 2019. [4](#)
- [14] Wenchao Du, Hu Chen, and Hongyu Yang. Learning invariant representation for unsupervised image restoration. In *Proceedings of the IEEE/CVF conference on computer vision and pattern recognition*, pages 14483–14492, 2020. [2](#)
- [15] Xinyu Jia, Chuang Zhu, Minzhen Li, Wenqi Tang, and Wenli Zhou. Lvip: A visible-infrared paired dataset for low-light vision. In *Proceedings of the IEEE/CVF International Conference on Computer Vision*, pages 3496–3504, 2021. [6](#)
- [16] Shahid Karim, Geng Tong, Jinyang Li, Akeel Qadir, Umar Farooq, and Yiting Yu. Current advances and future perspectives of image fusion: A comprehensive review. *Information Fusion*, 90:185–217, 2023. [1](#)
- [17] Junjie Ke, Qifei Wang, Yilin Wang, Peyman Milanfar, and Feng Yang. Musiq: Multi-scale image quality transformer. In *Proceedings of the IEEE/CVF international conference on computer vision*, pages 5148–5157, 2021. [6](#)
- [18] Boyi Li, Wenqi Ren, Dengpan Fu, Dacheng Tao, Dan Feng, Wenjun Zeng, and Zhangyang Wang. Benchmarking single-image dehazing and beyond. *IEEE Transactions on Image Processing*, 28(1):492–505, 2019. [2](#), [6](#)
- [19] Boyun Li, Xiao Liu, Peng Hu, Zhongqin Wu, Jiancheng Lv, and Xi Peng. All-In-One Image Restoration for Unknown Corruption. In *IEEE Conference on Computer Vision and Pattern Recognition*, New Orleans, LA, 2022. [8](#)
- [20] Boyun Li, Xiao Liu, Peng Hu, Zhongqin Wu, Jiancheng Lv, and Xi Peng. All-in-one image restoration for unknown corruption. In *Proceedings of the IEEE/CVF conference on computer vision and pattern recognition*, pages 17452–17462, 2022. [2](#), [4](#)
- [21] Bingchen Li, Xin Li, Yiting Lu, Ruoyu Feng, Mengxi Guo, Shijie Zhao, Li Zhang, and Zhibo Chen. Promptcir: blind compressed image restoration with prompt learning. In *Proceedings of the IEEE/CVF Conference on Computer Vision and Pattern Recognition*, pages 6442–6452, 2024. [2](#)
- [22] Hui Li and Xiao-Jun Wu. Densefuse: A fusion approach to infrared and visible images. *IEEE Transactions on Image Processing*, 28(5):2614–2623, 2018. [2](#), [6](#)
- [23] Hui Li and Xiao-Jun Wu. Crossfuse: A novel cross attention mechanism based infrared and visible image fusion approach. *Information Fusion*, 103:102147, 2024. [2](#)
- [24] Hui Li, Xiao-Jun Wu, and Tariq Durrani. Nestfuse: An infrared and visible image fusion architecture based on nest connection and spatial/channel attention models. *IEEE Transactions on Instrumentation and Measurement*, 69(12):9645–9656, 2020. [2](#)

- [25] Hui Li, Xiao-Jun Wu, and Josef Kittler. Mdlatrr: A novel decomposition method for infrared and visible image fusion. *IEEE Transactions on Image Processing*, 29:4733–4746, 2020. 2
- [26] Hui Li, Tianyang Xu, Xiao-Jun Wu, Jiwen Lu, and Josef Kittler. Lrrnet: A novel representation learning guided fusion network for infrared and visible images. *IEEE transactions on pattern analysis and machine intelligence*, 45(9):11040–11052, 2023. 1
- [27] Hui Li, Haolong Ma, Chunyang Cheng, Zhongwei Shen, Xiaoning Song, and Xiao-Jun Wu. Conti-fuse: A novel continuous decomposition-based fusion framework for infrared and visible images. *Information Fusion*, 117:102839, 2025. 2
- [28] Xin Li, Bingchen Li, Xin Jin, Cuiling Lan, and Zhibo Chen. Learning distortion invariant representation for image restoration from a causality perspective. In *Proceedings of the IEEE/CVF Conference on Computer Vision and Pattern Recognition*, pages 1714–1724, 2023. 3
- [29] Ziwen Li, Feng Zhang, Meng Cao, Jinpu Zhang, Yuanjie Shao, Yuehuan Wang, and Nong Sang. Real-time exposure correction via collaborative transformations and adaptive sampling. In *Proceedings of the IEEE/CVF Conference on Computer Vision and Pattern Recognition*, pages 2984–2994, 2024. 7
- [30] Pengwei Liang, Junjun Jiang, Xianming Liu, and Jiayi Ma. Fusion from decomposition: A self-supervised decomposition approach for image fusion. In *European Conference on Computer Vision*, pages 719–735. Springer, 2022. 1
- [31] Jinyuan Liu, Xin Fan, Zhanbo Huang, Guanyao Wu, Risheng Liu, Wei Zhong, and Zhongxuan Luo. Target-aware dual adversarial learning and a multi-scenario multi-modality benchmark to fuse infrared and visible for object detection. In *Proceedings of the IEEE/CVF Conference on Computer Vision and Pattern Recognition*, pages 5802–5811, 2022. 2, 6
- [32] Jiayi Ma, Wei Yu, Pengwei Liang, Chang Li, and Junjun Jiang. Fusionsgan: A generative adversarial network for infrared and visible image fusion. *Information fusion*, 48:11–26, 2019. 2
- [33] Jiayi Ma, Hao Zhang, Zhenfeng Shao, Pengwei Liang, and Han Xu. Ganmcc: A generative adversarial network with multiclassification constraints for infrared and visible image fusion. *IEEE Transactions on Instrumentation and Measurement*, 70:1–14, 2020. 2
- [34] Liye Mei, Xinglong Hu, Zhaoyi Ye, Linfeng Tang, Ying Wang, Di Li, Yan Liu, Xin Hao, Cheng Lei, Chuan Xu, et al. Gtmfuse: Group-attention transformer-driven multi-scale dense feature-enhanced network for infrared and visible image fusion. *Knowledge-Based Systems*, 293:111658, 2024. 6, 7
- [35] Anish Mittal, Rajiv Soundararajan, and Alan C Bovik. Making a “completely blind” image quality analyzer. *IEEE Signal processing letters*, 20(3):209–212, 2012. 6
- [36] Hanseok Oh, Hyunji Lee, Seonghyeon Ye, Haebin Shin, Hansol Jang, Changwook Jun, and Minjoon Seo. Instructir: A benchmark for instruction following of information retrieval models. *arXiv preprint arXiv:2402.14334*, 2024. 5, 6
- [37] Yohan Poirier-Ginter and Jean-François Lalonde. Robust unsupervised stylegan image restoration. In *Proceedings of the IEEE/CVF Conference on Computer Vision and Pattern Recognition*, pages 22292–22301, 2023. 3
- [38] Alec Radford, Jong Wook Kim, Chris Hallacy, Aditya Ramesh, Gabriel Goh, Sandhini Agarwal, Girish Sastry, Amanda Askell, Pamela Mishkin, Jack Clark, et al. Learning transferable visual models from natural language supervision. In *International conference on machine learning*, pages 8748–8763. PmLR, 2021. 4
- [39] J Wesley Roberts, Jan A Van Aardt, and Fethi Babikker Ahmed. Assessment of image fusion procedures using entropy, image quality, and multispectral classification. *Journal of Applied Remote Sensing*, 2(1):023522, 2008. 6
- [40] Christos Sakaridis, Dengxin Dai, and Luc Van Gool. Semantic foggy scene understanding with synthetic data. *International Journal of Computer Vision*, 126:973–992, 2018. 2
- [41] Linfeng Tang, Jiteng Yuan, Hao Zhang, Xingyu Jiang, and Jiayi Ma. Piafusion: A progressive infrared and visible image fusion network based on illumination aware. *Information Fusion*, 2022. 2, 6
- [42] Wei Tang, Fazhi He, Yu Liu, Yansong Duan, and Tongzhen Si. Datfuse: Infrared and visible image fusion via dual attention transformer. *IEEE Transactions on Circuits and Systems for Video Technology*, 33(7):3159–3172, 2023. 2
- [43] Alexander Toet. Tno image fusion dataset. *figshare*, 2024. 6
- [44] Hugo Touvron, Thibaut Lavril, Gautier Izacard, Xavier Martinet, Marie-Anne Lachaux, Timothée Lacroix, Baptiste Rozière, Naman Goyal, Eric Hambro, Faisal Azhar, et al. Llama: Open and efficient foundation language models. *arXiv preprint arXiv:2302.13971*, 2023. 6
- [45] Jiayi Wang, Kelvin CK Chan, and Chen Change Loy. Exploring clip for assessing the look and feel of images. In *Proceedings of the AAAI conference on artificial intelligence*, pages 2555–2563, 2023. 6
- [46] Wu Wang, Liang-Jian Deng, Ran Ran, and Gemine Vivone. A general paradigm with detail-preserving conditional invertible network for image fusion. *International Journal of Computer Vision*, pages 1–26, 2023. 6, 7
- [47] Xintao Wang, Liangbin Xie, Chao Dong, and Ying Shan. Real-esrgan: Training real-world blind super-resolution with pure synthetic data. In *Proceedings of the IEEE/CVF international conference on computer vision*, pages 1905–1914, 2021. 2
- [48] Xue Wang, Zheng Guan, Wenhua Qian, Jinde Cao, Runzhuo Ma, and Cong Bi. A degradation-aware guided fusion network for infrared and visible image. *Information Fusion*, 118:102931, 2025. 2, 6, 8
- [49] Zhou Wang and Alan C Bovik. A universal image quality index. *IEEE signal processing letters*, 9(3):81–84, 2002. 6
- [50] Zhou Wang, Eero P Simoncelli, and Alan C Bovik. Multiscale structural similarity for image quality assessment. In *The Thirty-Seventh Asilomar Conference on Signals, Systems & Computers*, 2003, pages 1398–1402. Ieee, 2003. 6

- [51] Chen Wei, Wenjing Wang, Wenhan Yang, and Jiaying Liu. Deep retinex decomposition for low-light enhancement. *arXiv preprint arXiv:1808.04560*, 2018. 2, 6
- [52] Wenhui Wu, Jian Weng, Pingping Zhang, Xu Wang, Wenhan Yang, and Jianmin Jiang. Uretinex-net: Retinex-based deep unfolding network for low-light image enhancement. In *Proceedings of the IEEE/CVF conference on computer vision and pattern recognition*, pages 5901–5910, 2022. 7
- [53] Enze Xie, Wenhai Wang, Zhiding Yu, Anima Anandkumar, Jose M Alvarez, and Ping Luo. Segformer: Simple and efficient design for semantic segmentation with transformers. *Advances in neural information processing systems*, 34: 12077–12090, 2021. 8
- [54] Han Xu, Jiayi Ma, Zhuliang Le, Junjun Jiang, and Xiaojie Guo. Fusiondn: A unified densely connected network for image fusion. In *proceedings of the Thirty-Fourth AAAI Conference on Artificial Intelligence*, 2020. 2, 6
- [55] Sidi Yang, Tianhe Wu, Shuwei Shi, Shanshan Lao, Yuan Gong, Mingdeng Cao, Jiahao Wang, and Yujiu Yang. Maniqa: Multi-dimension attention network for no-reference image quality assessment. In *Proceedings of the IEEE/CVF Conference on Computer Vision and Pattern Recognition*, pages 1191–1200, 2022. 6
- [56] Xunpeng Yi, Han Xu, Hao Zhang, Linfeng Tang, and Jiayi Ma. Text-if: Leveraging semantic text guidance for degradation-aware and interactive image fusion. In *Proceedings of the IEEE/CVF Conference on Computer Vision and Pattern Recognition*, pages 27026–27035, 2024. 1, 2, 5, 6, 8
- [57] Syed Waqas Zamir, Aditya Arora, Salman Khan, Munawar Hayat, Fahad Shahbaz Khan, and Ming-Hsuan Yang. Restormer: Efficient transformer for high-resolution image restoration. In *Proceedings of the IEEE/CVF conference on computer vision and pattern recognition*, pages 5728–5739, 2022. 2, 4, 5
- [58] Hao Zhang, Han Xu, Xin Tian, Junjun Jiang, and Jiayi Ma. Image fusion meets deep learning: A survey and perspective. *Information Fusion*, 76:323–336, 2021. 1
- [59] Lvmin Zhang, Anyi Rao, and Maneesh Agrawala. Adding conditional control to text-to-image diffusion models. In *Proceedings of the IEEE/CVF international conference on computer vision*, pages 3836–3847, 2023. 5
- [60] Weixia Zhang, Guangtao Zhai, Ying Wei, Xiaokang Yang, and Kede Ma. Blind image quality assessment via vision-language correspondence: A multitask learning perspective. In *IEEE Conference on Computer Vision and Pattern Recognition*, pages 14071–14081, 2023. 6
- [61] Zeyang Zhang, Hui Li, Tianyang Xu, Xiao-Jun Wu, and Josef Kittler. Ddbfusion: An unified image decomposition and fusion framework based on dual decomposition and bézier curves. *Information Fusion*, 114:102655, 2025. 1
- [62] Wenda Zhao, Shigeng Xie, Fan Zhao, You He, and Huchuan Lu. Metafusion: Infrared and visible image fusion via meta-feature embedding from object detection. In *Proceedings of the IEEE/CVF Conference on Computer Vision and Pattern Recognition*, pages 13955–13965, 2023. 2
- [63] Zixiang Zhao, Haowen Bai, Jianshe Zhang, Yulun Zhang, Shuang Xu, Zudi Lin, Radu Timofte, and Luc Van Gool. Cddfuse: Correlation-driven dual-branch feature decomposition for multi-modality image fusion. In *Proceedings of the IEEE/CVF conference on computer vision and pattern recognition*, pages 5906–5916, 2023. 2
- [64] Zixiang Zhao, Haowen Bai, Yuanzhi Zhu, Jianshe Zhang, Shuang Xu, Yulun Zhang, Kai Zhang, Deyu Meng, Radu Timofte, and Luc Van Gool. Ddfm: denoising diffusion model for multi-modality image fusion. In *Proceedings of the IEEE/CVF International Conference on Computer Vision*, pages 8082–8093, 2023. 2
- [65] Zixiang Zhao, Jiang-She Zhang, Haowen Bai, Yicheng Wang, Yukun Cui, Lilun Deng, Kai Sun, Chunxia Zhang, Junmin Liu, and Shuang Xu. Deep convolutional sparse coding networks for interpretable image fusion. In *CVPR Workshops*, pages 2369–2377. IEEE, 2023. 6, 7, 8